University of Venda

Investigation of the synthesis and characterization of $Li_2M(SO_4)_2$ where M = Cu, Cr or V for lithium-ion batteries

A thesis submitted to the Department of Chemistry in fulfilment of the requirements for the degree

MSc in Chemistry

by

Mahandana Ndivhuho Anita

Student number: 11521016

School of Mathematical and Natural Sciences

UNIVERSITY OF VENDA

THOHOYANDOU, LIMPOPO

SOUTH AFRICA

Supervisor(Dr M.A. Legodi): Date:……

Co-supervisor (Prof. T. van Ree): Date:.....

February 2021

Abstract

Many researchers have put their efforts in developing various types of sulphate-based cathode materials for lithium-ion batteries such as $Li_2Co(SO_4)_2$, $Li_2Mn(SO_4)_2$, $Li_2Fe(SO_4)_2$ and many others. This study focuses on the synthesis and characterization of three compounds of the $Li_2M(SO_4)_2$ family, where M = Cu, Cr, or V. The three compounds were successfully synthesized using sol-gel and solid-state (ball milling) methods. All compounds were characterized using FTIR, XRD, SEM, and four-point probe instruments. All synthesized compounds correspond to cubic structures according to Bragg's law. $Li_2Cu(SO_4)_2$ and $Li_2VO(SO_4)_2$ are conductive under sol-gel method with 2.3 V and 0.16 V. Some on the compounds synthesised have shown structures under SEM, with pores which have small diameters which is a requirement for the pore size in lithium-ion batteries.

Keywords: lithium-ion batteries, ball milling method, sol-gel method.

Declaration

I, Ndivhuho Anita Mahandana, declare that this dissertation is my original work and has not been submitted for any other degree at any other University or tertiary Institution. The proposal does not contain other persons' writing unless specifically acknowledged and referenced accordingly.

Signed (Student): Mahandana N A Date: 11/02/2021

Mahandana Ndivhuho Anita

Dedication

This research is dedicated to my husband (Mr. Nekhubvi VM), my parents (Mr & Mrs. Mahandana), my daughter (Lutendo), my son (Mulinda), and my siblings (Thifhelimbilu, Noretta, Ndidinwangani, Nthambeleni & Adivhaho) for their love, motivation, and support.

Acknowledgements

Firstly, I would like to thank Jehovah for the protection, wisdom, and perseverance he gave me to complete this dissertation.

I would also like to thank my supervisor Dr Legodi M.A. and co-supervisor Prof. T. van Ree for guidance, patience, motivation, and availability whenever I needed assistance.

I wish to express my sincere gratitude and appreciation to all staff members of the Department of Chemistry.

Not forgetting my colleagues, Abigail, and Rudzani for the encouragement to complete this MSc degree.

My Uncle and all my friends who encouraged me to further my studies.

Lastly, I would like to thank Dr Legodi's research group for the assistance, CSIR, and the University of Pretoria for analyzing the samples.

Symbols and Abbreviations

$CuSO_4$	Copper sulphate
Li_2CrSO_4	Dilithium chromium sulphate
$Li_2Cu(SO_4)_2$	Dilithium copper disulphate
$Li_2Fe(SO_4)_2$	Dilithium iron disulphate
$Li_2Mn(SO_4)_2$	Dilithium manganese disulphate
Li_2SO_4	Dilithium sulphate
$Li_2VO(SO_4)_2$	Dilithium vanadyl disulphate
FTIR	Fourier transform infrared
IR	Infrared
LIBs	Lithium-ion batteries
XRD	Powder X-ray diffraction
SEM	Scanning electron microscope

List of Figures

List of Tables

Table of Contents

Chapter 1

Introduction

The increase in demand for enhanced energy-storage devices, from small application batteries to bigger ones for grid applications has propelled research in electrochemical sciences in the last decades (Schwieger *et al*., 2011; Oliveira *et al*., 2015). Rechargeable lithium-ion batteries remain one of the most durable power applications ranging from watt-hours to gigawatt-hours (Chen *et al*., 2018).

Batteries have been interesting products for decades but today it looks like they may become even more important, more especially lithium metal and lithium-ion batteries (Dewulf *et al*., 2010). Lithium-ion batteries (LIBs) provide an unmatched combination of high energy density, high voltage, high power density, fast charging / discharging properties and environmental friendliness (Xi *et al*., 2015; Nitta *et al*., 2015; Iizuka *et al*., 2013; Chen *et al*., 2018). All these properties make LIBs the technology of choice for portable electronics, power tools, and hybrid or full electric vehicles.

The reduced lifetime of electronic products due to the development of the latest technologies results in the generation of large volumes of electronic waste. This includes components that contain valuable metals like lithium and cobalt. The rapid consumption rate of lithium-ion batteries is an indication of environmental hazards at the end of life unless it is recycled properly (Prabaharan *et al*., 2017). Recycling spent LIBs is beneficial not only for metal recovery but also for protecting the environment and conserving primary resources (Prabaharan *et al*., 2017). Since some of the batteries are difficult to degrade, it is not wise to dispose of them in the municipal waste (Al-thyabat *et al*., 2013). The best way is to recycle them; however, little is known about recycling LIBs from consumer electronics in many countries like China. The leakage of organic electrolytes as well as heavy metals will lead to serious soil contamination if the spent LIBs are directly dumped into landfills

(Gu *et al*., 2017). Lessons learned from recycling lead-acid batteries can be used to tailor-make new environmental policies to ensure all recyclable materials in the spent batteries are recycled and not sent to the landfills (Mayyas *et al*., 2018).

As the demand for portable electronic equipment is growing rapidly, the production and consumption of the batteries is also increasing very quickly (Jha *et al*., 2013). New challenges of developing high-performance energy storage devices for electric vehicle and grid storage technologies have led to the emergence of lithium-containing polyanion framework compounds as candidates for next-generation cathode materials (Radha *et al*., 2015). Lithium-ion batteries have certain advantages over others since Li has the lowest reduction potential of all metals, so that Li based batteries have the highest possible cell potential (Mayyas *et al*., 2018). Lithium is also the third lightest element and has one of the smallest ionic radii of any single-charged ion, which endows Li-based batteries with high gravimetric and volumetric capacities and high-power density (Nitta *et al*.,2015).

A range of $Li_2M(SO_4)_2$ mixed salts has been obtained in monoclinic marinate $Li_2M(SO_4)_2$ (M = Mg, Mn, Fe, Co) and orthorhombic $Li_2M(SO_4)_2$ (M = Fe, Co, Zn, Ni) forms. These polymorphic forms were synthesized using solid-state ceramic processing for the monoclinic phase and ball milling for the orthorhombic phase (Clark *et al*., 2014). The present study will extend the recent study of Clark *et al*. (2014) by synthesizing and characterizing $Li_2M(SO_4)_2$ using methods employed in synthesizing $Li_2Fe(SO_4)_2$.

Coating is one of the effective and controllable approaches to stabilize the electrode interface and reduce side reactions. Several coating materials can be used, for example carbon materials, metals, oxides, phosphates, lithium compounds, polymers, etc. Carbon coating is known to increase the conductivity of the insulating materials and to protect the electrode from direct contact with the electrolyte, which results in good rate capabilities (Yi *et al*., 2016).

$Li_2Cu_2O(SO_4)_2$ and $Li_2VO(SO_4)_2$ have been previously synthesized (Reynaud, 2014). Both were synthesized using a ball milling method under an argon environment and calcinated over the temperature interval 400 – 500 °C. The results for $Li_2Cu_2O(SO_4)_2$ showed that the redox activity of Cu^{3+}/Cu^{2+} was approximately 4.7 V vs Li^+/Li° with a limited capacity of 20 mAh/g. On the other hand, $Li_2VO(SO_4)_2$ was found to have a redox potential of 4.75 V with a capacity of approximately 60 mA.h/g after 10 cycles.

1.1 Problem statement

- The use of lithium-ion batteries has increased over the past decades for use in electronic devices which suggests that its composition should be made from affordable and environmentally friendly materials. However, there still a challenge to develop high-performance energy storage devices.
- Therefore, research on lithium-containing polyanion framework compounds as candidates for next-generation cathode materials will probably make a difference.
- Out of the existing metals in the $Li_2M(SO_4)_2$ family for use in lithium-ion batteries copper is not yet in use and is cheap compared to some of the previously utilized metals, for example M = Ni, Mn, etc.
- Attempting to measure the cell voltage will advance the research on this family.

1.2 Aim of the study

- To synthesize and characterize $Li_2M(SO_4)_2$, where M = Cu, Cr, or V, as cathode material for use in lithium-ion batteries.

1.3 Objectives of the study

- To synthesize $Li_2Cu(SO_4)_2$, Li_2CrSO_4 and $Li_2VO(SO_4)_2$ using sol-gel and solid state methods

- To characterize the synthesized compounds using FTIR, PXRD, SEM and four-point probe resistivity measurements
- To compare the results of sol-gel and solid-state synthesis methods
- To measure the conductivity of the synthesized compounds

Chapter 2

Literature Review

Several previous researchers worked on developing cathode material for rechargeable lithium-ion batteries, but the safety problem is still an issue due to Li metal dendrites depositing during the charging process (Satyavani *et al*., 2015), causing short-circuits. In the early 1970s, the first lithium battery based on $Li/Li^+/Li_xTiS_2$ technology was withdrawn from the market due to the formation of lithium dendrites which short-circuited the cell. Twenty years later, in 1991, a new generation of Li-ion batteries was commercialized by Sony Corporation. Since 1999, a serious search for new iron-based polyanionic compounds displaying enhanced Fe^{3+}/Fe^{2+} redox voltages (Lander *et al.*, 2014) was initiated. This research resulted in the discovery of new polyanionic compounds, such as borates and silicates, which display higher capacities but present lower redox voltages of approximately 2.8 V vs Li^+/Li^o. Currently, mainly Japanese, Korean, and Chinese companies are manufacturing lithium-ion batteries in bulk.

The metallic lithium anode was replaced by graphite, which could reversibly intercalate lithium. However, the problem with graphite as an electrode is that it has a low theoretical capacity and poor capability, which cannot satisfy the requirements of high-energy-efficient next-generation energy storage systems (Ma *et al*., 2015). It is therefore crucial to develop new alternative electrode materials that will have higher reversible capacity and desirabley rate capability for the next generation of lithium-ion batteries.

There exist several studies focussing on $Li_2M(SO_4)_2$ in the literature. Radha *et al*.-(2015) determined the enthalpies of formation of $Li_2M(SO_4)_2$ (M = Mn, Fe, Co, and Ni) for both monoclinic and orthorhombic phases. For the orthorhombic phase, ball milling was employed and for the monoclinic phase a solid-state (ceramic) method was employed. This study was conducted to understand thermodynamic driving forces behind phase stability and transformation behaviour of this new class

of materials. Results showed that the enthalpies of dissolution of monoclinic phases are less exothermic compared to orthorhombic phases for Fe- and Co-based $Li_2M(SO_4)_2$ samples. This suggests that the monoclinic phases are more stable than their orthorhombic counterparts. However, electrochemical properties were not determined in this study.

Clark *et al*. (2014) investigated key issues related to defects chemistry, lithium diffusion, surface structures, and voltage trends of monoclinic samples $Li_2M(SO_4)_2$ (M = Mn, Fe, Co) as in the study of Radha *et al.* (2015). They used density-functional theory, a computational modeling method, to investigate the electronic structure. They have calculated morphology of $Li2Fe(SO_4)_2$ which was rhombohedral-like shape with (011) and (210) surfaces. The computed cell voltage was 3.99 V, which was reasonable when compared to the experimentally measured voltage of 3.83 V.

Lander *et al*. (2016) successfully synthesized the family of bimetallic sulfates $A_2M(SO_4)_2$ with A = Li, Na and M = Mn, Fe, Co, Ni, Zn. Especially the monoclinic marinite $Li_2Fe(SO_4)_2$ phase generated great interest due to its high Fe^{3+}/Fe^{2+} redox potential. They also proved the existence of polymorphism within the $Li_2M(SO_4)_2$ phases, with the $Li_2M(SO_4)_2$ (M = Fe, Co, Ni, Zn) compounds. They were able to crystallize these compounds in an orthorhombic structure (Figure 1) by changing the synthetic conditions, i.e. use of a ball milling route as opposed to the ceramic route for the monoclinic polymorphs (Figure 2).

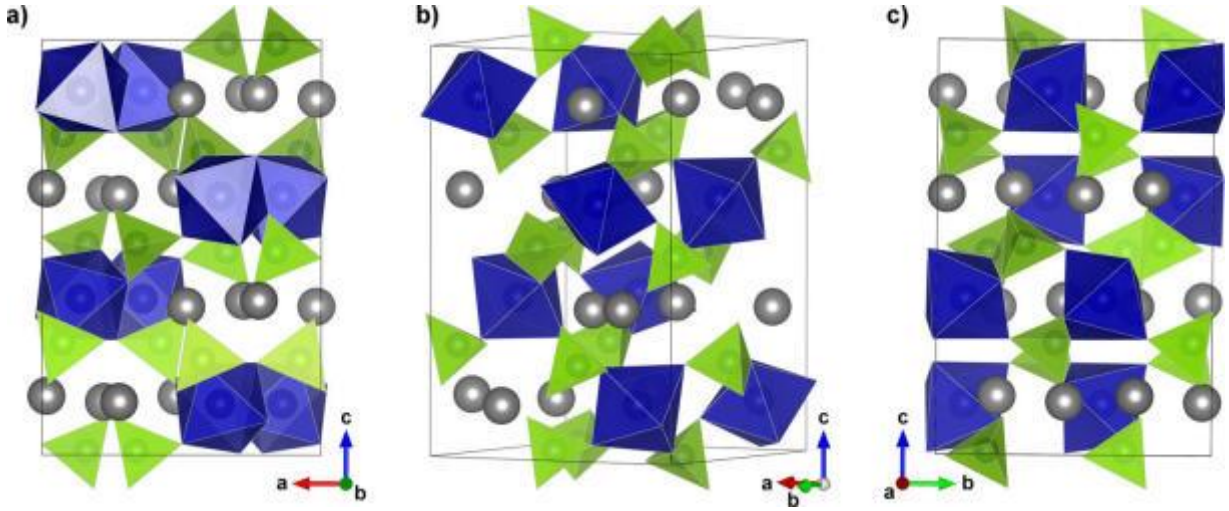

Figure 1: The orthorhombic structures of the $Li_2M(SO_4)_2$ (M = Co, Fe, Zn, Ni, Mg) phases [Lander et al. (2016)]

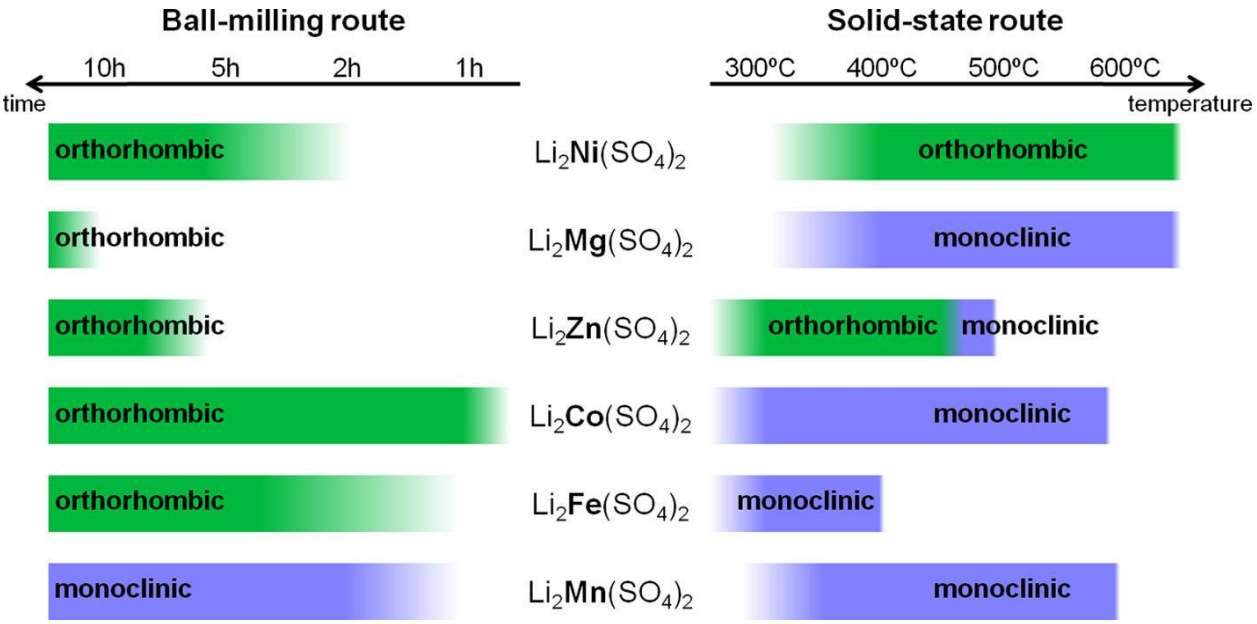

Figure 2: Schematic diagram summarizing the nature of the $Li_2M(SO_4)_2$ polymorph [Lander et al. (2014)]

Reynaud *et al*. (2014) recently showed the feasibility of replacing the $(PO_4)^{3-}$ polyanion by the more electronegative $(SO_4)^{2-}$ to increase the redox potential from 3.45 V ($LiFePO_4$) to 3.83 V for $Li_2Fe(SO_4)_2$.

Based on these observations, the main focus of the present study is the synthesis and characterization of mixed lithium metal sulphates with selected metals for use as cathode materials in lithium-ion batteries, i.e. $Li_2M(SO_4)_2$ where M = Cr, Cu or V. Although numerous studies, as discussed in the above paragraphs, have reported the synthesis of $Li_2M(SO_4)_2$ where M = Mn, Fe, Co, Ni, Zn, etc., there is a lack of information on the synthesis and properties of $Li_2Cu(SO_4)_2$, initiating the present investigation.

Chapter 3

Experimental Methods

For this study the methodology (Reynaud, 2014) employed for the synthesis of $Li_2Fe(SO_4)_2$ was used to prepare samples of $Li_2Cu(SO_4)_2$, $Li_2VO(SO_4)_2$, and Li_2CrSO_4. Two synthesis methods were, namely a solid-state and sol-gel method.

3.1 Sol-gel method

Stoichiometric amounts of Li_2SO_4 and $CuSO_4.5H_2O$ were weighed and mixed (Liu *et al*., 2004). The mixture was then divided into two samples each weighing 5 g. Each 5 g of the sample was then dissolved in 50 ml distilled water. Starch (3,5 g) was added to the solution while stirring with a magnetic stirrer for about 20 minutes to make a homogeneous solution. This solution was heated on a hotplate between 70 °C and 80 °C while stirring until the gel precursor was formed. The gel precursor was then heated in an oven at 120 °C for 3 h to remove excess water to form a dry gel. This method was also employed for the mixtures of Li_2SO_4 with $VOSO_4$ and CrO_3, respectively. The dry gel for each compound was then calcined at 500°C for 3 h and 7 h, respectively, in a furnace. To obtain a polycrystalline product, the product was crushed using a mortar and pestle. All samples were prepared for further investigation using FTIR, XRD, SEM, and four-point probe resistivity instruments.

3.2 Solid-state method

$CuSO_4.5H_2O$ and $VOSO_4.xH_2O$ were first dehydrated at 270 °C for a few hours to obtain anhydrous $CuSO_4$ and $VOSO_4$, respectively (Laura, 2016).

The stoichiometric amounts of Li_2SO_4 and $CuSO_4$ were weighed and then ground using a mortar and pestle. The mixture was then divided into 2 samples. One sample was calcined at 500 °C for 3 h and the other was calcined at 500 °C for 7 h. To obtain a polycrystalline product, the samples were ground again using a mortar and pestle. This method was also employed for the mixtures of Li_2SO_4

with $VOSO_4$ and CrO_3, respectively. All samples were prepared for further investigation using FTIR, XRD, SEM, and four-point probe resistivity instruments.

3.3 Instrumental Analysis

3.3.1 Solid-State Fourier-Transform-Infrared Spectroscopy (FTIR)

FTIR is a technique utilized to obtain a spectrum of absorption or emission of a solid, liquid, or gas. An FTIR spectrometer was simultaneously used to collects high-spectral-resolution data over a wide spectral range. This confers a significant advantage over a dispersive spectrometer, which measures intensity over a narrow range of wavelength at a time (Griffiths & de Hasseth, 2007). It consists of a source, interferometer, sample holder, detector, amplifier, A/D converter, and a computer. The model which we used was Alpha Bruker FTIR spectrometer with the computer installed with Opus software. The sample is placed on the sample holder. The source produces radiation which passes through the interferometer and reaches the detector; the output is transferred to the computer in the form of spectra. All samples were analysed at 16 °C to produce the most accurate measurements.

3.3.2 Powder X-Ray diffraction (XRD)

XRD is one of a number of analytical techniques that use X-ray, neutron, or electron diffraction on powder for structural characterization of material (Cullity, 1978). It examines the purity and crystallinity of material (Qiao *et al*., 2009). A Bruker model D8 Advance diffractometer and Lynxeye XE detector was used to collect the powder XRD patterns of the prepared $Li_2M(SO_4)_2$. The XRD patterns were recorded for 1 hour in the 2θ range of 5 - 90°. To obtain the XRD patterns of $Li_2M(SO)_4$, the samples were subjected to XRD for analysis at 40 mA and 40 kV with a scan axis 2θ and wavelength of 1.544426 Å. To get more accurate data the samples were ground to a size of 1 mm pellets. The prepared pellets were then placed in the appropriate sample holder and then inserted

into the X-ray diffractometer. The X-rays generated was directed onto the flat surface of the sample and the elements at that surface then diffract the X-ray beam at appropriate angles. The results are in the form of a plot of angle vs X-ray intensity obtained from the sample.

3.3.3 Scanning electron microscopy (SEM)

An SEM is a type of microscope used to produce images of a sample by scanning the sample surface with a focused beam of electrons. The electrons interact with atoms in the sample produced to produce various signals that contain information regarding the surface topography and the composition of the sample. The electron beam is scanned in a raster scan pattern, and the position of the beam is combined with the intensity of the detected signal to produce an image (Stokes, 2008).

3.3.4 Four-point probe resistivity tester

Four-point probes are routinely used for semiconductor material characterization. Most commonly they measure the sheet resistance of thin conducting layers and wafers. Their advantage, compared to the two-point probe, lies in the way the current and voltage are measured (Valdes, 1954; Chandra *et al*., 2011). The two outermost electrodes serve as current injector and collector, while the resulting voltage drop is measured with no current fashion via the inner electrodes. This method practically eliminates measurement errors due to contact resistance between the electrodes and the sample (Petersen *et al*., 2002). A high current is used to supply current through the outer two probes, a voltmeter then measures the voltage across the inner two probes to determine the resistivity. All samples were first compressed to a thickness of 1 mm (1000 micron) before being analysed. The instrument used consists of a Signatone stand with 4-point head, connected to an HP3245A current source with HP34970 acquisition/voltmeter. Measurements are then taken with a Labview program.

Chapter 4

Results and Discussion

4.1 FTIR results

The various FTIR stretching and bending absorption bands were recorded for $Li_2M(SO_4)_2$ where M = Cu, Cr, and V. The FTIR spectra are shown in Figures 3 to 14. The absorption band at 410.27 cm^{-1} in Figure 3 indicates the stretching vibration for the Li-O bond. The bands at 608.43 and 1611.79 cm^{-1} indicate O-H bending. The band at 1098.84 cm^{-1} indicates the stretching vibrations of SO_4^{2-}. The C-O stretching band appears at 1611.70 cm^{-1} (Chang & Huang, 1998).

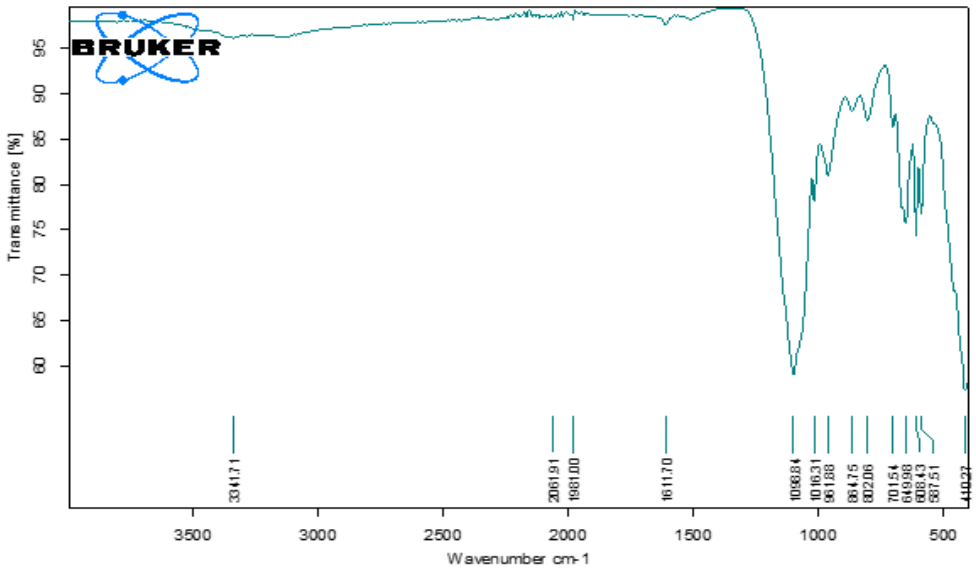

Figure 3: FTIR spectrum of $Li_2Cu(SO_4)_2$ calcined at 500 ^oC for 3 h, solid-state method

The absorption at 616.75 cm^{-1} in Figure 4 indicates the O-H bending. Wavenumber 1094.28 cm^{-1} indicates the stretching of SO_4^{2-}, C-O Stretching Band. 1610.96 cm^{-1} indicates O-H bending (Chang and Huang, 1998).

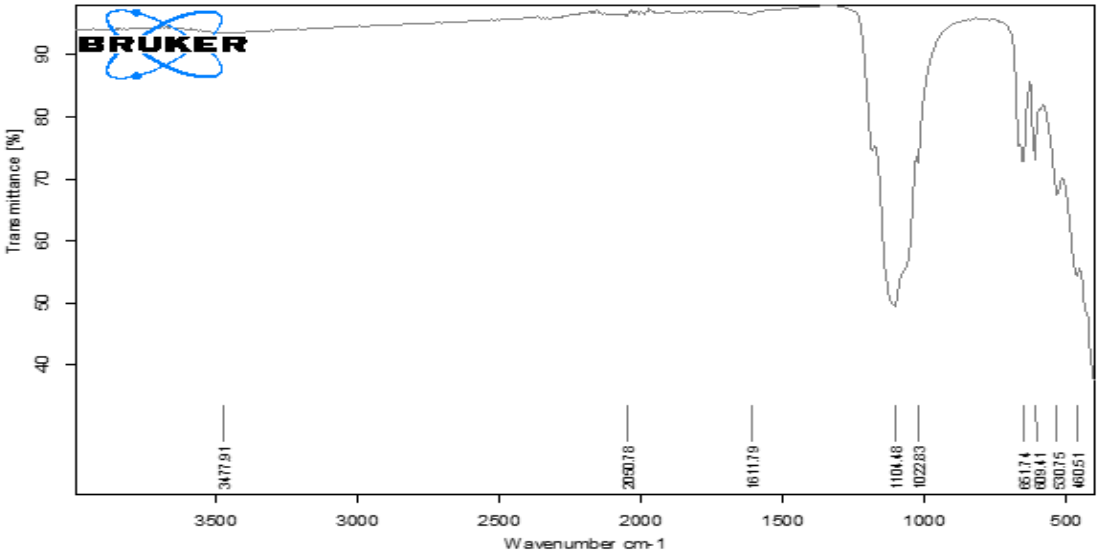

Figure 4: FTIR spectrum of $Li_2Cu(SO_4)_2$ calcined at 500°C for 3 h, sol-gel method

The IR band at 460.51 cm^{-1} in Figure 5 indicates the stretching absorption band for Li-O. The IR band at 651.74 cm^{-1} indicates the O-H bending. Wavenumbers 1104.48 cm^{-1} and 1102.81 cm^{-1} indicate the stretching of SO_4^{2-}, C-O stretching. Band 1611.79 cm^{-1} indicates O-H bending (Chang and Huang, 1998).

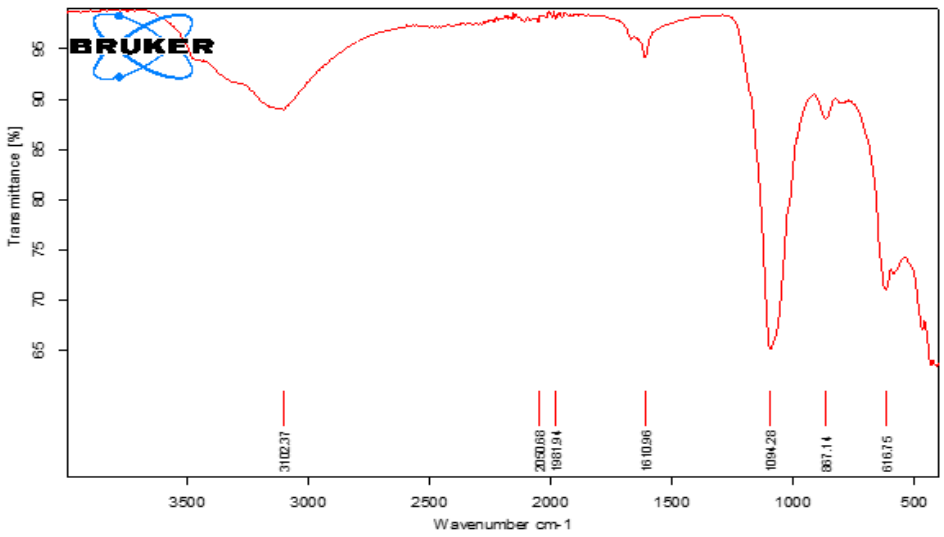

Figure 5: FTIR spectrum of $Li_2Cu(SO_4)_2$ calcined at 500 °C for 7 h using solid-state method

The IR band at 651.12 cm^{-1} in Figure 6 indicates the O-H bending. Wavenumber 1102.81 cm^{-1} indicates the stretching of SO_4^{2-}, C-O stretching due to starch. Band at 1631.48 cm^{-1} indicates O-H bending (Chang and Huang, 1998).

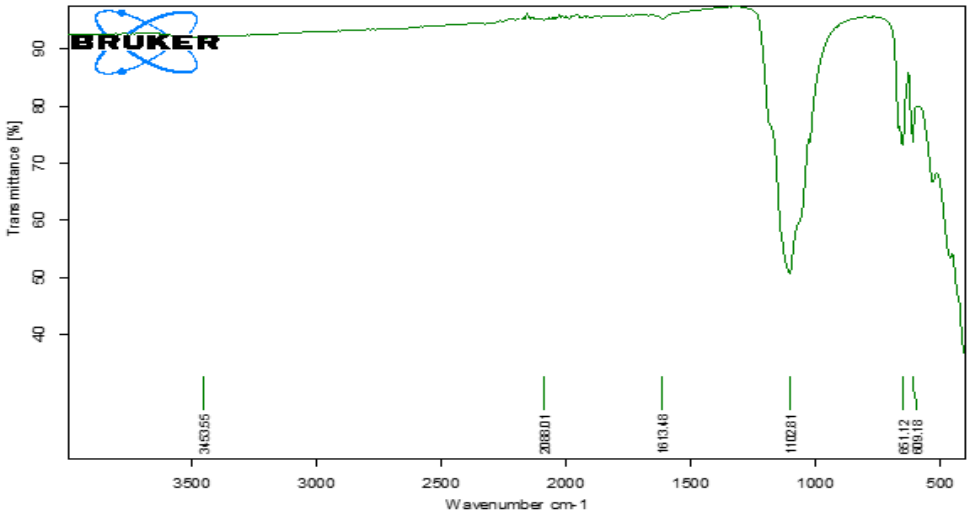

Figure 6: FTIR spectrum of $Li_2Cu(SO_4)_2$ calcined at 500 ^oC for 7 h using sol-gel method

The band between 441.26 and 531.76 cm^{-1} in Figure 7 indicates that the recovered product contains Cr_2O_3 crystals. The band at 531.76 cm^{-1} indicates the stretching of SO_4. Band at 609.48 cm^{-1}, indicates Cr-O stretching. Band at 111.42 cm^{-1} shows the vibration of SO_4^{2-} ions. Band at 1613.17 cm^{-1} indicates the bending of water (Chen *et al*., 2004; Levason *et al*., 2014).

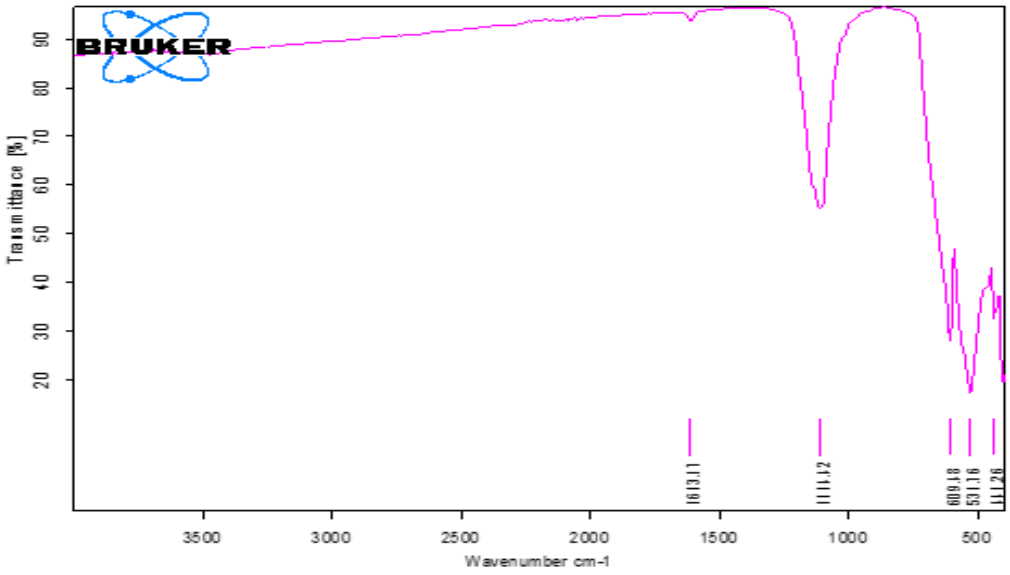

Figure 7 : FTIR spectrum of Li_2CrSO_4 calcined at 500 ^oC for 3 h using a solid-state method

The band between 441.51 and 532.38 cm^{-1} in Figure 8 indicates that the recovered product contains Cr_2O_3 crystals. The band at 532.38 cm^{-1} indicates the stretching of SO_4. Band at 612.58 cm^{-1} indicates Cr-O stretching. Band at 1096.96 cm^{-1} shows the vibration of SO_4 ions. Band at 1610.72 cm^{-1} indicates the bending of water. This FTIR results indicate that we have successfully synthesized Li_2CrSO_4 (Chen *et al*., 2004; Levason *et al*., 2014).

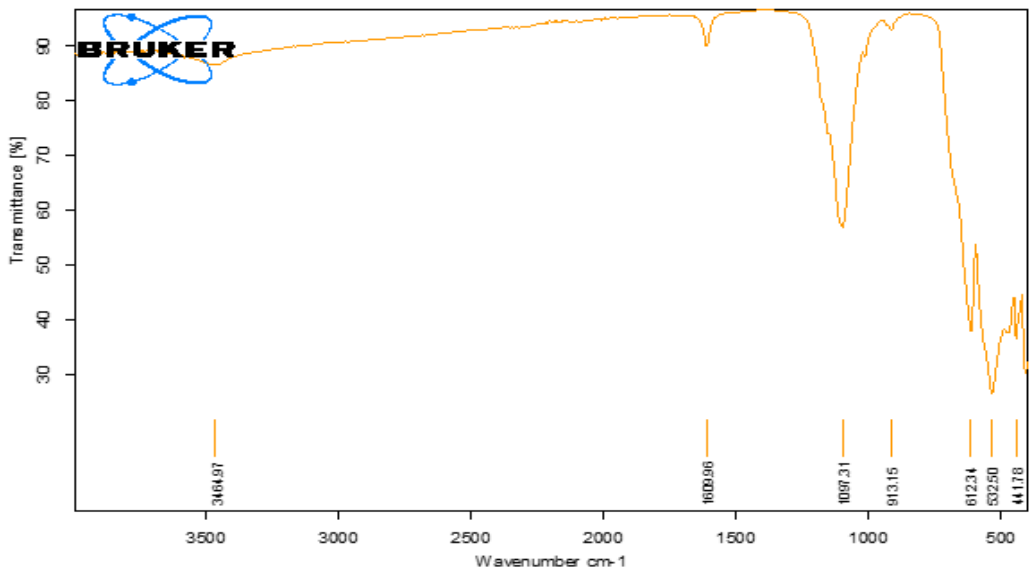

Figure 8: FTIR spectrum of Li_2CrSO_4 calcined at 500 ^oC for 3 h using sol-gel method

The band at 532.50 cm^{-1} in Figure 9 indicates the stretching of SO_4. Band at 612.34 cm^{-1} indicates Cr-O stretching. Band at 1097.31 cm^{-1} shows the vibration of SO_4^{2-} ions. Band 1609.96 cm^{-1} indicates the bending of water. These FTIR results show that Li_2CrSO_4 was successfully synthesized (Chen *et al*., 2004; Levason *et al*., 2014).

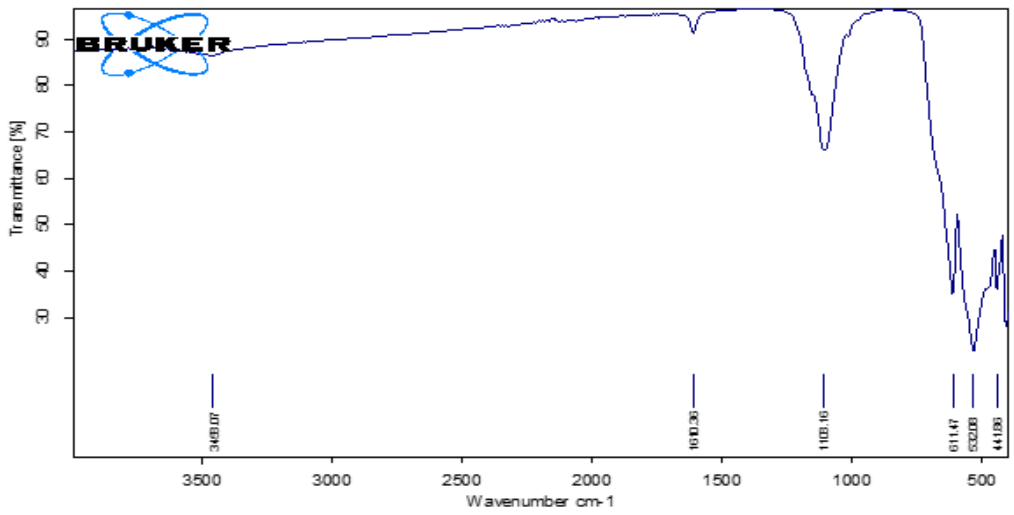

Figure 9: FTIR spectrum of Li_2CrSO_4 calcined at 500 ^oC for 7 h solid-state method

The band at 533.33 cm^{-1} in Figure 10 indicates the stretching of SO_4. Band at 612.54 cm^{-1} indicates Cr-O stretching. Band at 1097.02 cm^{-1} shows the vibration of SO_4^{2-} ions. Band at 1610.25 cm^{-1} indicates the bending of water (Chen *et al*., 2004; Levason *et al*., 2014).

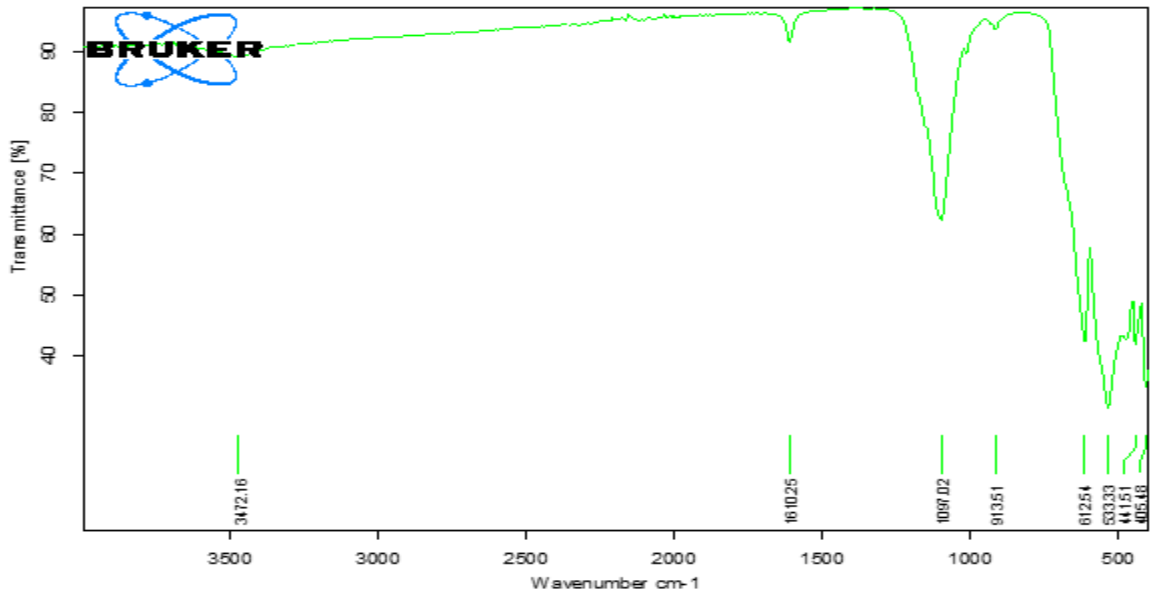

Figure 10: FTIR spectrum of Li_2CrSO_4 calcined at 500 ^oC for 7 h sol-gel method

The vibration between 935.05 - 1001.27 cm^{-1} in Figure 11 indicates the V=O vibration. The band at 1096.63 cm^{-1} indicates the vibration mode of sulphate ions. The band at 1610.96 cm^{-1}, indicates the water bending (Guimond *et al*., 2006; Doadrio *et al.,* 2002).

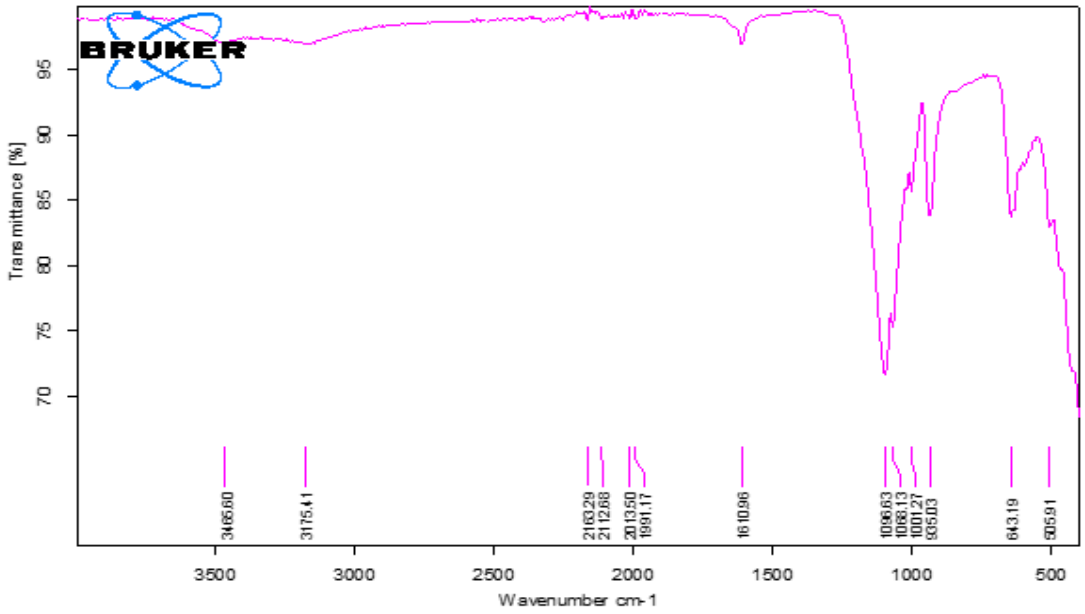

Figure 11: FTIR spectrum of $Li_2VO(SO_4)_2$ calcined at 500 ^oC for 3 h solid-state method

The vibration between 979.84 - 1011.06 cm^{-1} in Figure 12 indicates the V=O vibration. The band between 1614.58 cm^{-1} indicates the water bending (Guimond *et al*., 2006; Doadrio *et al*., 2002).

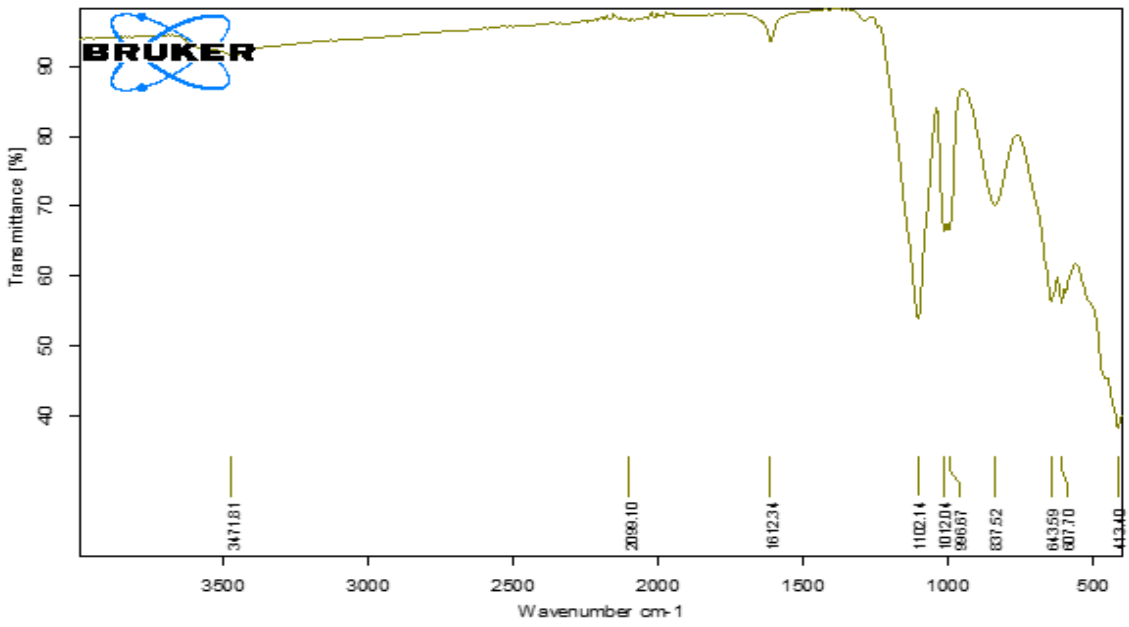

Figure 12: FTIR spectrum of $Li_2VO(SO_4)_2$ calcined at 500 ^oC for 3 h sol-gel method

The vibration between 1012.04 cm^{-1} in Figure 13 indicates the V=O. The band at 1102.14 cm^{-1} indicates the vibration mode of sulphate ions. The band 1612.34 cm^{-1} indicates the water bending.

The band at 1102.14 cm^{-1} indicates the C-O bond due to the presence of starch and the band at 413.40 cm^{-1} indicates the presence of Li-O (Guimond *et al*., 2006; Doadrio *et al*., 2002).

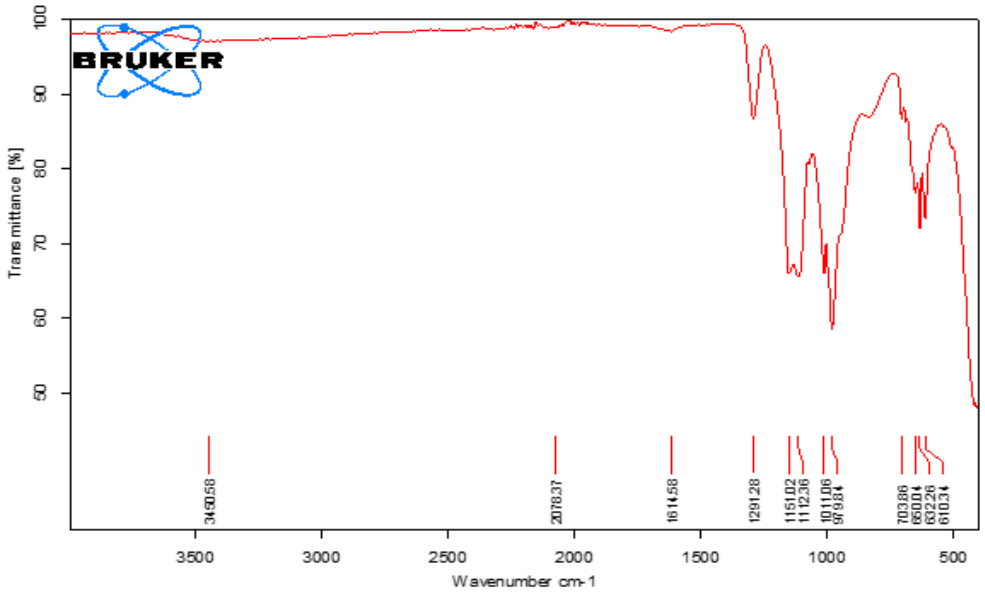

Figure 13: FTIR spectrum of $Li_2VO(SO_4)_2$ calcined at 500 ^oC for 7 h solid-state method

The vibration 1011.92 cm^{-1} in Figure 14 indicates the V=O vibration. The band at 1100.88 cm^{-1} indicates the vibration mode of sulphate ions. The band at 1611.08 cm^{-1} indicates the water bending. The band at 1100.88 cm^{-1} indicates the C-O bond due to the presence of starch under the sol-gel method. Wavenumber around 410.45 cm^{-1} indicates the presence of Li-O (Guimond *et al*., 2006; Doadrio *et al*., 2002).

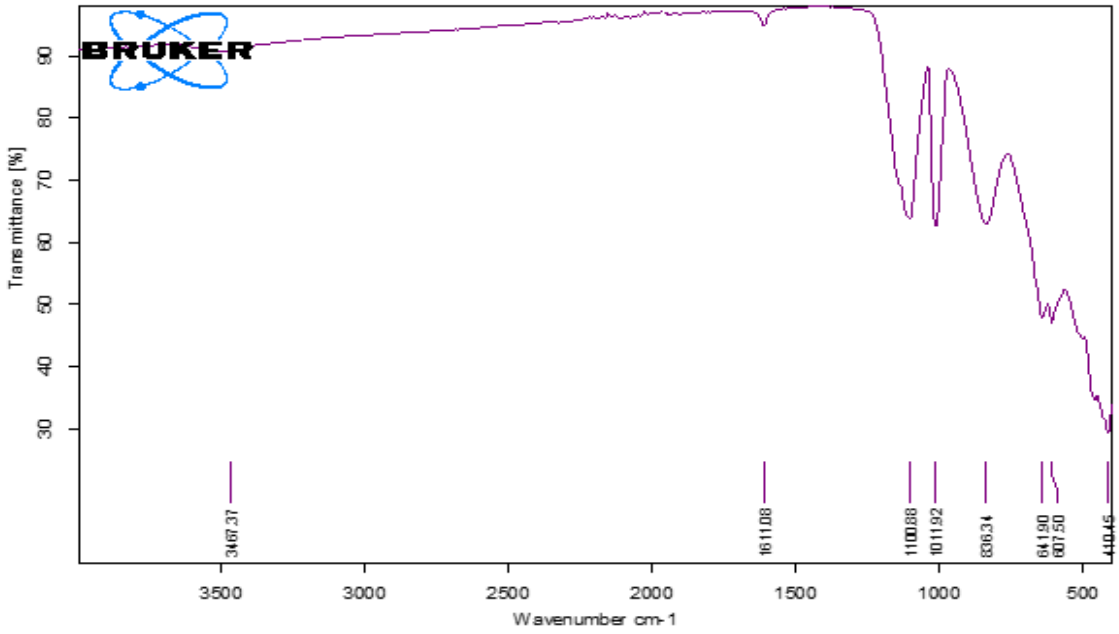

Figure 14: FTIR spectrum of $Li_2VO(SO_4)_2$ calcined at 500 ^oC for 7 h sol-gel method

The IR spectroscopy results shows that the targeted compounds were successfully synthesised because in all samples there are relevant functional groups present. Both methods were successfu.

A summary of the FTIR results is shown in Tables 1, 2, and 3 in the Appendix.

4.2 XRD results

The XRD spectra of the prepared samples are shown in Figures 15 to 20. The peak indexes were calculated using Bragg's law (Theivasanthi & Alagar, 2010). From the information in Figure 15, the interplanar spacing was calculated using Bragg's law i.e. $n\lambda = 2d\sin\theta$, where λ = wavelength of X-ray, d = interplanar spacing, θ = diffraction angle and n = 1. The value of d for $Li_2VO(SO_4)_2$ was calculated as 0.206 nm. The unit cell dimensions were calculated for a cubic system geometry, i.e. FCC (Face centered cubic lattice), $\alpha = 2r\sqrt{2}$ where *r* is the atomic radius. The atomic radius of the vanadium is 0.205 nm. Therefore, α = 0.580 nm. From the available information, it can be concluded that the diffraction peak at 2θ = 44° corresponds to the (300) crystal plane, which denotes a primitive cubic structure (Khan *et al*., 2016). Refer to Table 4 in the Appendix section for further information.

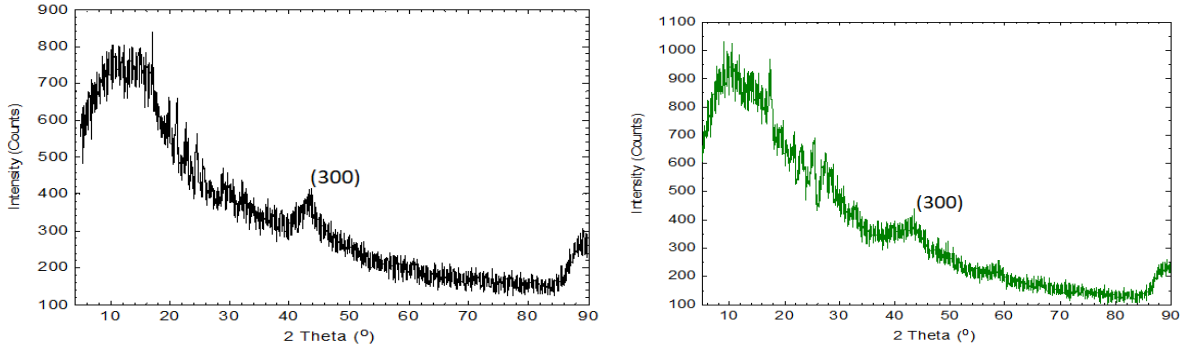

(a) **(b)**

Figure 15: XRD spectrum of $Li_2VO(SO_4)_2$ calcined at 500 °C for 3 h by (a) sol-gel and (b) solid-state method

In Figure 16a, there is a diffraction peak at 2θ = 44° that corresponds to the (300) crystal plane. In Figure 16b, there is also a diffraction peak at 2θ = 44°, which also corresponds to the crystal plane of (300). Both methods produced a primitive cubic structure (Khan *et al*., 2016).

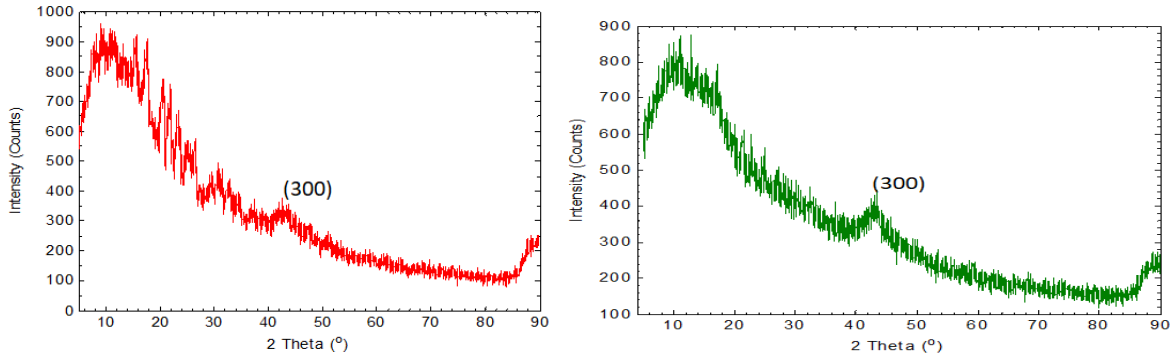

(a) **(b)**

Figure 16: XRD spectra of $Li_2VO(SO_4)_2$ calcined at 500 °C for 7 h by (a) sol-gel and (b) solid-state method

In Figure 17a, there are diffraction peaks at 2θ = 42° and 54° which correspond to the (200) crystal plane which is a body-centered cubic structure. In Figure 17b, there are diffraction peaks at 2θ = 36° and 42°, which correspond to the crystal planes (100) and (200), respectively. Crystal plane (100) denotes a simple cubic structure and crystal plane (200) represents a body-centered cubic structure (Khan *et al*., 2016).

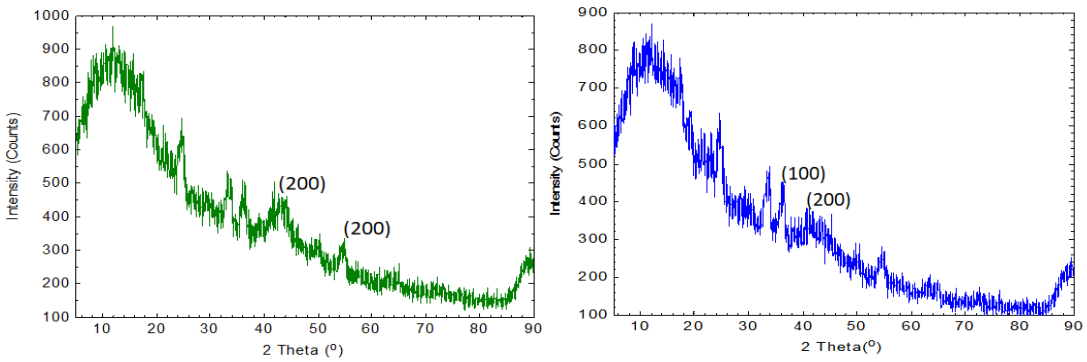

(a) **(b)**

Figure 17: XRD spectra of $Li_2Cr(SO_4)_2$ calcined at 500 °C for 3 h by (a) sol-gel and (b) solid-state method

In Figure 18a, there are diffraction peaks at 2θ = 44° and 54° which both correspond to the (200) crystal plane. In Figure 18b there is a diffraction peak at 2θ = 54° that also corresponds to the (200) crystal plane. Both methods have shown the body-centered cubic structure (Khan *et al*., 2016).

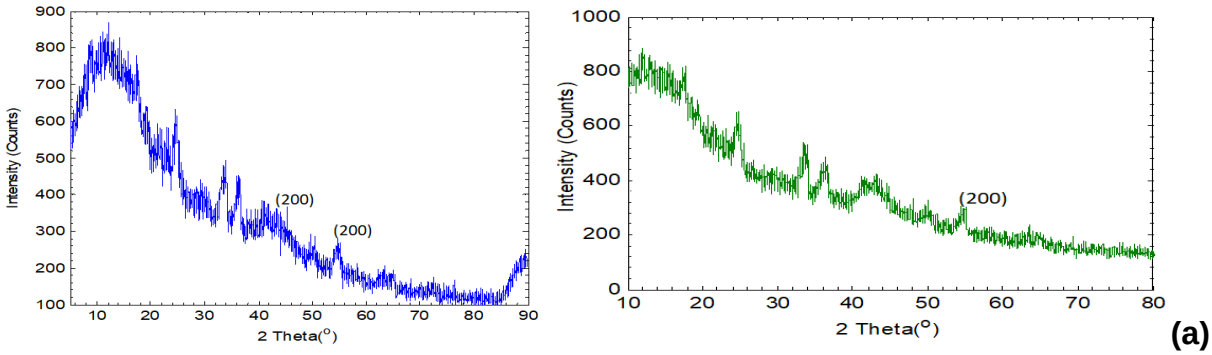

(a)

(b)

Figure 18: XRD spectra of $Li_2Cr(SO_4)_2$ calcined at 500 °C for 7 h by (a) sol-gel and (b) solid-state method

In Figure 19a there is a diffraction peak at 2θ = 40° which corresponds to the (200) crystal plane of a body-centered cubic structure. In Figure 19b no diffraction peak is observed. This might have been caused by the presence of mostly amorphous material.

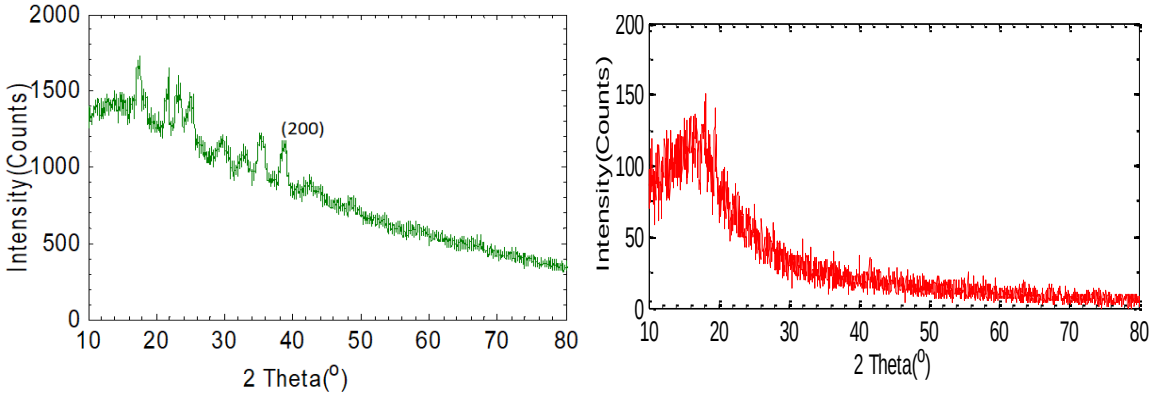

(a) **(b)**

Figure 19: XRD spectrum of $Li_2Cu(SO_4)_2$ calcined at 500 °C for 3 h by (a) sol-gel and (b) solid-state method

In Figure 20a there is a diffraction peak at 2θ = 40° which corresponds to the (200) crystal plane of a body-centered cubic structure. In Figure 20b no relevant diffraction peaks were observed. This might have been caused by unknown substances present.

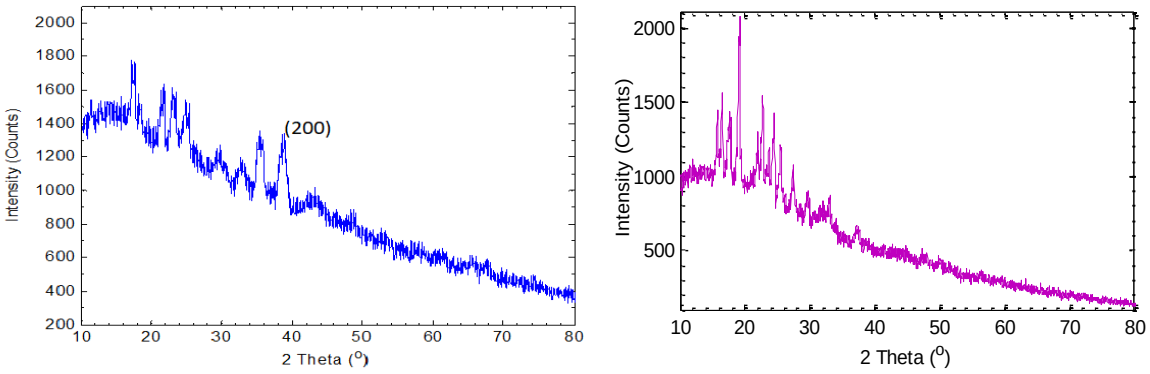

(a) **(b)**

Figure 20: XRD spectrum of $Li_2CuSO_4)_2$ calcined at 500 °C for 7 h by (a) sol-gel and (b) solid-state method

The XRD spectra of both $Li_2VO(SO_4)_2$ and Li_2CrSO_4 have crystalline pattern since they have sharp peaks for both synthetic methods. $Li_2Cu(SO_4)_2$ shows the amorphous pattern on the solid state method because of the absence of sharp peaks. Crystalline pattern is visible under sol-gel method of $Li_2Cu(SO_4)_2$. The reason might be that in sol-gel method starch was used as a chelating ligand and the reactants were dissolved in distilled water whereas under solid state method, only the reactants were mixed together. The amorphous pattern may have also been caused by the impurities. In future, EDS (Energy-dispersive X-ray spectroscopy) will be used to identify these unknown substances (Khan *et al*., 2016). The solid state method seems to be less useful because some samples produced broad diffraction peaks at 2θ value less than 40°. The results obtained using the sol-gel method were more acceptable because the samples are more crystalline and crystallinity plays a good role on the performance of LIBs (Zhuang *et al*., 2020). A summary of XRD results is given in Table 4 in the Appendix.

4.3 Scanning Electron Microscope (SEM) results

In Figure 21-26 images of the calcinated powders for both methods are shown. The particle shapes and morphologies were evaluated using scanning electron microscopy (SEM). Particles in all samples show non-uniform size distributions (Figures 21 to 26) where the magnification was at 5000. Looking at SEM images in figure 21 (a) representing $Li_2Cu(SO_4)_2$ calcinated at 500 for 7 h by solid state and SEM images in figure 23 (a), representing $Li_2VO(SO_4)_2$ calcinated at 500 for 7h by solid state we see grains which are in good contact with each other. It is evident from the images recorded that some contains pores structure, and some do not have. Those with pore structures have small diameters which is a requirement for the pore size in lithium-ion batteries, as this prevent dendric lithium penetration from occurring during the consecutive battery life (Kovachev et al., 2019). This shows that calcination time influences the size of the particles. (Kusuma & Chandrappa, 2019). The particle sizes for all sol-gel method products were also smaller than those produced by the solid-state method in all figures mentioned below.

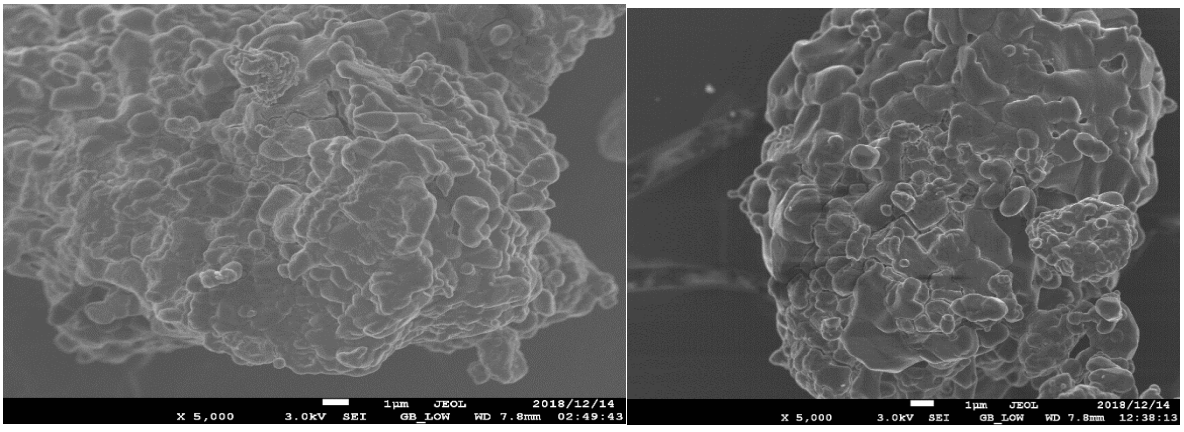

(a) **(b)**

Figure 21: SEM representation of $Li_2Cu(SO_4)_2$ calcined at 500 ^oC for 7 h by (a) solid-state and (b) sol-gel method

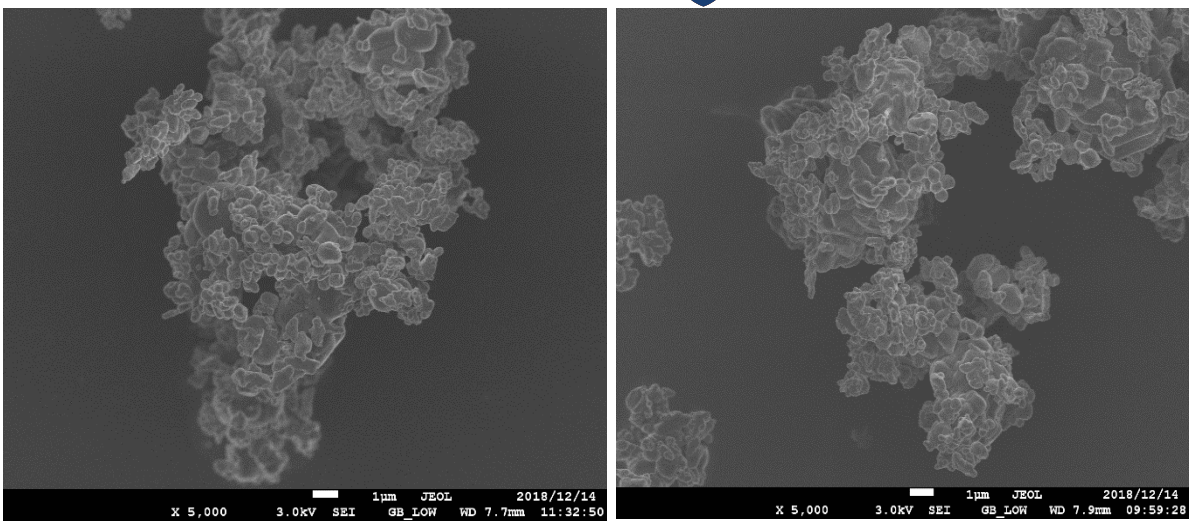

(a) **(b)**

Figure 22 : SEM Representation of Li_2CrSO_4 calcined at 500 °C for 7 h by (a) solid-state and (b) sol-gel method

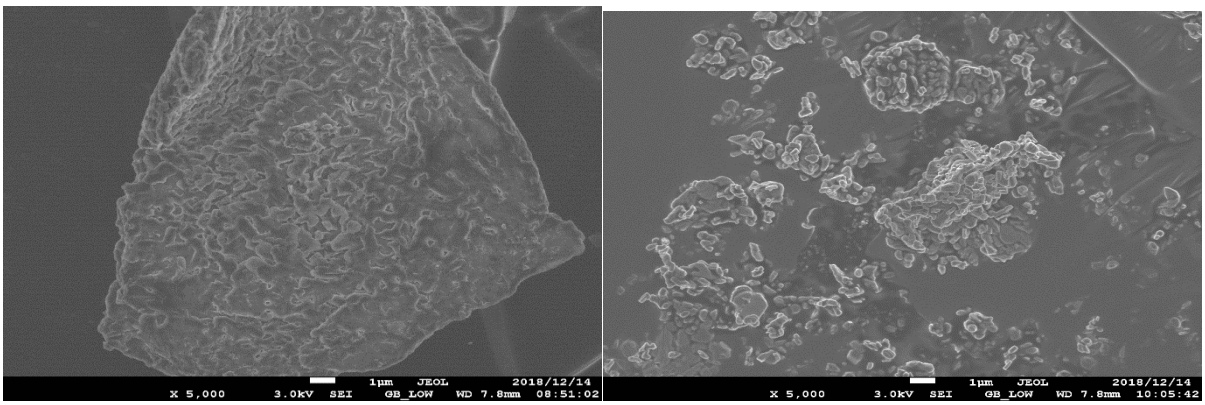

(a) **(b)**

Figure 23: SEM Representation of $Li_2VO(SO_4)_2$ calcined at 500 °C for 7 h by (a) solid-state and (b) sol-gel method

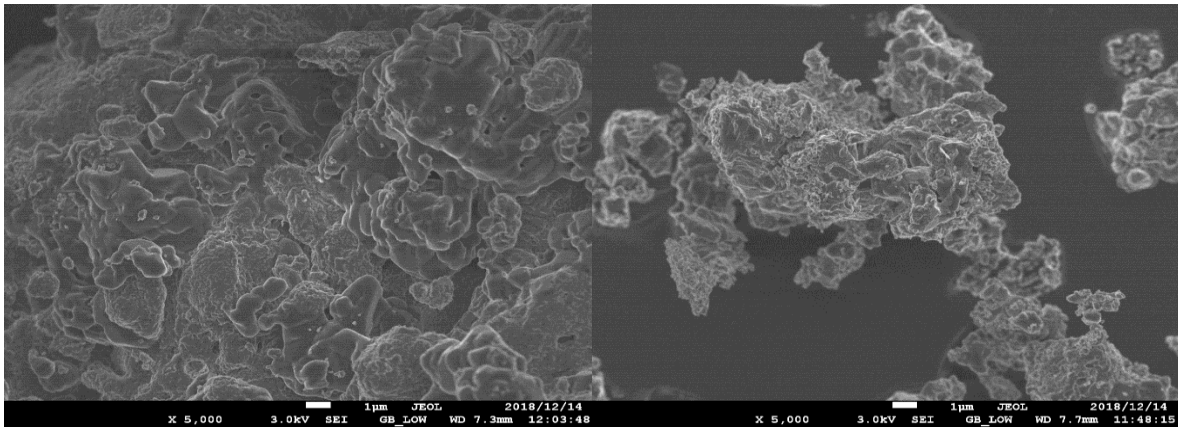

(a) **(b)**

Figure 24: SEM representation of $Li_2Cu(SO_4)_2$ calcined at 500 °C for 3 h by (a) solid-state and (b) sol-gel method

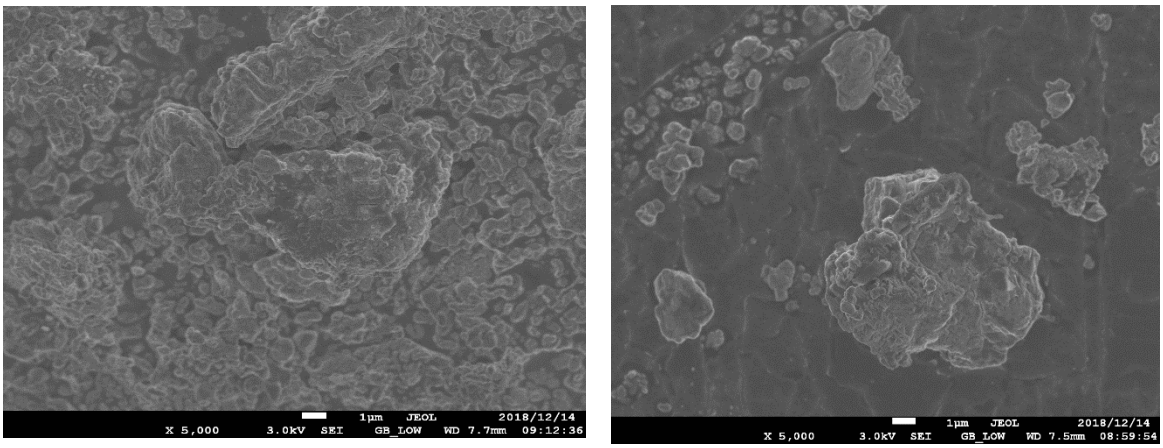

(a) **(b)**

Figure 25: SEM representation of Li_2CrSO_4 calcined at 500 °C for 3 h by (a) solid-state and (b) sol-gel method

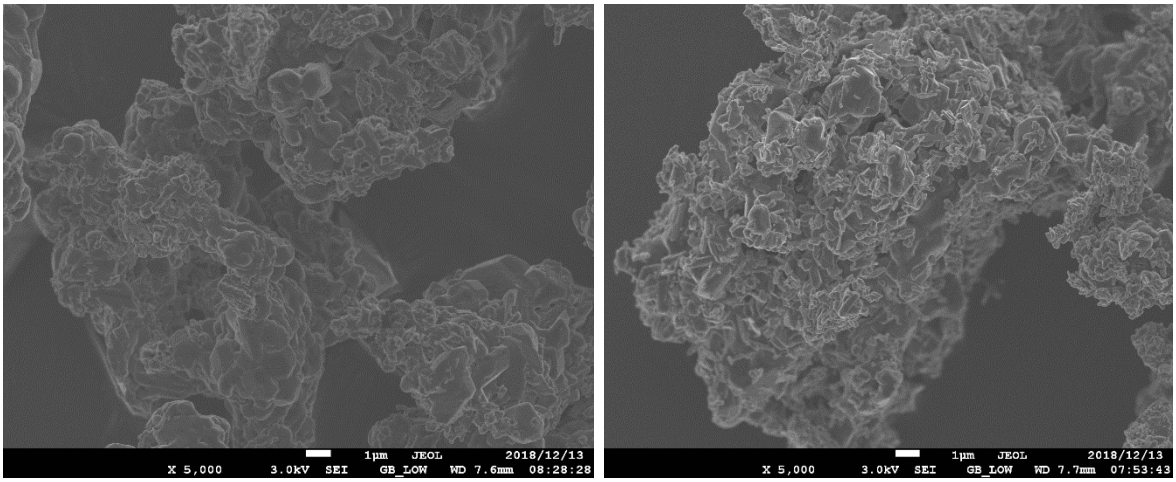

Figure 26: SEM representation of $Li_2VO(SO_4)_2$ calcined at 500 °C for 3 h by (a) solid-state and (b) sol-gel method

4.4 Four-probe semi-conductor results

Carbon coating was used on all samples mainly to effectively improve the conductivity and protecting the direct contact of the electrode with the electrolyte. (Yi *et al.*, 2016). All 12 samples were

characterized using four-probe semi-conductor testing for conductivity. Only two samples have shown conductivity. The results are shown in Figures 27– 29.

The graph in Figure 27 shows a good agreement of the current versus voltage with $R^2 = 0.9360$ and the voltage was ranging from 1.8 - 2.3 V. This result shows that $Li_2Cu(SO_4)_2$ is electrochemically active.

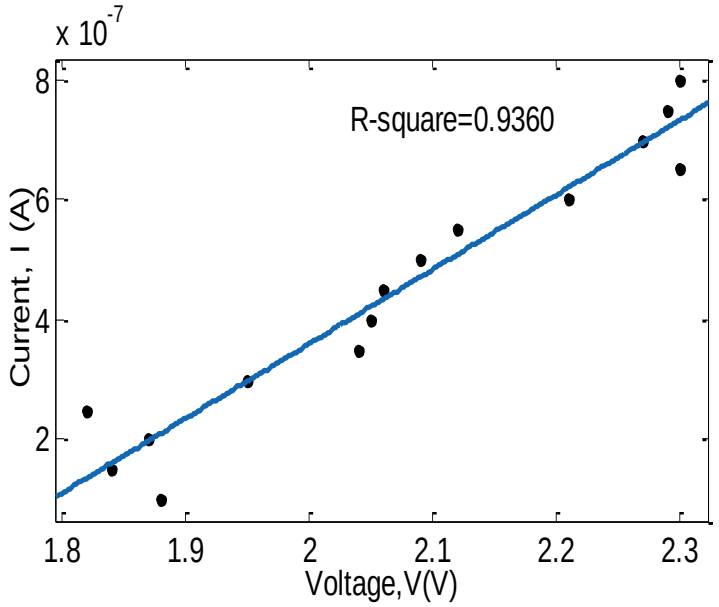

Figure 27: Current vs Voltage graph of $Li_2Cu(SO_4)_2$ calcined at 500 ^oC for 7 h (sol-gel method) measured with a four-point probe

The graph in Figure 28 shows a good agreement of the relationship of current versus voltage with $R^2 = 0.9989$ and the voltage was ranging 0.02 - 016 V. This result shows that $Li_2VO(SO_4)_2$ is electrochemically active. For $Li_2VO(SO_4)_2$ the electrical resistivity before measurements of current and voltage was 55955.2039 Ω.cm.

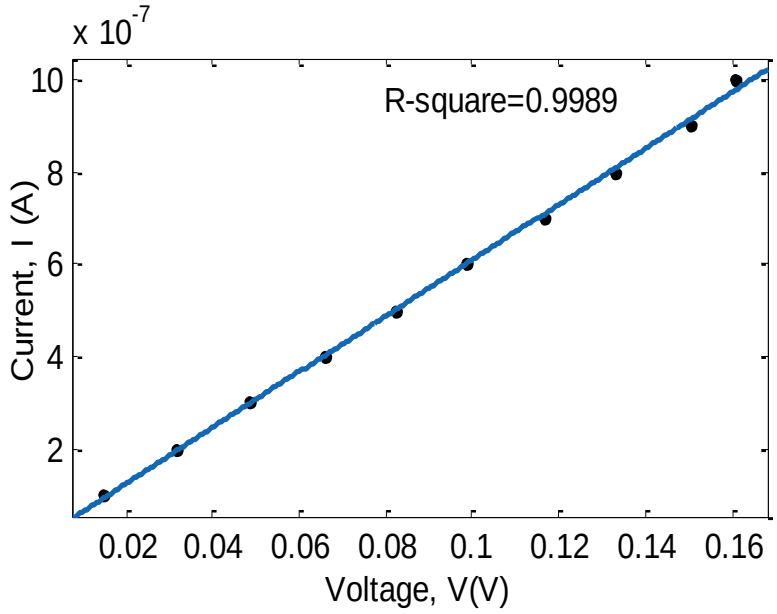

Figure 28: Current vs Voltage graph of $Li_2VO(SO_4)_2$ calcined at 500 °C for 7 h measured with a four-point probe (sol-gel method)

The graph in Figure 29 does not show a good agreement of the relationship of current and voltage with $R^2 = 0.6137$ because of the higher resistivity which makes the results obtained to be unreliable. For Li_2CrSO_4, the electrical resistivity before measurements of current and voltage was 1438583.389 Ω.cm.

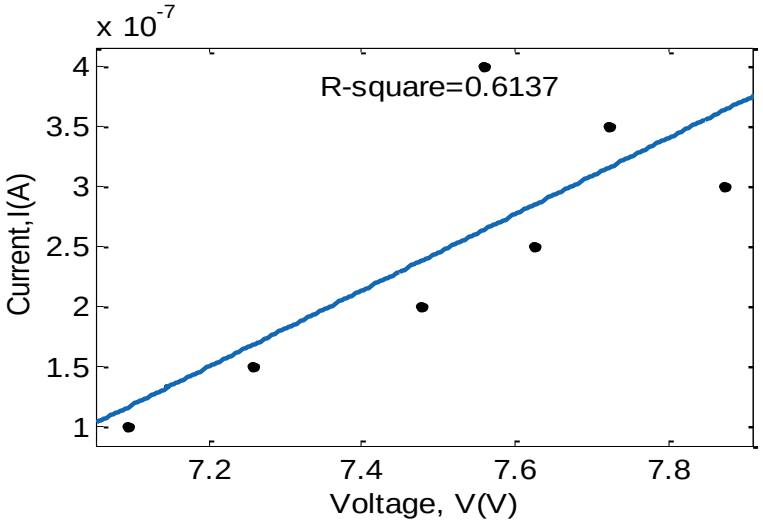

Figure 29: Current vs Voltage graph of Li_2CrSO_4 calcined at 500 °C for 7 h measured with a four-point probe (solid-state method)

Chapter 5

Conclusions and future scope

$Li_2(CuSO_4)_2$, Li_2CrSO_4, and $Li_2VO(SO_4)_2$ were successfully synthesized by both sol-gel and solid-state method. The FTIR results confirmed that the expected compounds were synthesised based on the presence of relevant bonds of each sample for both sol-gel and solid-state method. XRD patterns showed diffraction peaks for all samples except for $Li_2Cu(SO_4)_2$ synthesized by solid-state method, calcined at 500 °C for 3 h and 7 h. This indicates that $Li_2Cu(SO_4)_2$ synthesized by the solid-state method is not crystalline which might have been affected by the dehydrating period or presence of impurities. Miller indices (*hkl*) were also calculated using Bragg's law, for $Li_2VO(SO_4)_2$ value of *hkl* was (300), Li_2CrSO_4 the value of *hkl* (200) and (200) for $Li_2Cu(SO_4)_2$.

The surface morphology of the samples was also studied by SEM analysis and the results indicated non-uniform distribution for the sample. It was also determined that the shapes of the synthesized materials are cubic, and the particle size of all samples synthesized using the sol-gel method was smaller as compared to samples synthesized by the solid-state method. Out of 12 samples characterized using the four-point probe semi-conductor instrument, only 2 samples $Li_2Cu(SO_4)_2$ calcined at 500 °C for 7 h and $Li_2VO(SO_4)_2$ calcined at 500 °C for 3 h) show a good relationship between current and voltage because the resistivity is low. They were both synthesized via sol-gel method. All other samples showed high electrical resistivity. The high electrical resistivity prevented electrical conductivity through the synthesized products, which is the reason there was no good relationship between current and voltage. We can conclude in this study that sol-gel method worked better than the solid-state method. In this regard, we also expect that cathode materials synthesized via sol-gel will be more electrochemically active than those from solid state methods because of their better conductivity.

To extend the present study, there is a need to improve the electrical conductivity of $Li_2Cu(SO_4)_2$ and $Li_2VO(SO_4)_2$ by doping with other materials, also the use of different annealing temperature for different time intervals may be useful. We will subject $Li_2Cu(SO_4)_2$ and $Li_2VO(SO_4)_2$ to other electrochemical tests for example, cycling performance, charge and discharge curves, etc. We will also do Rietveld refinement and crystal parameter calculations. We will also try and use other chelating agents like nitric acid or citric acid instead of starch to test if there will be an improvement in the outcomes of the samples. We will also try to find other sources of Cr so that we can synthesize $Li_2M(SO_4)_2$ M = Cr again to see if there would be an improvement in the results. Lastly, we will try different methods of synthesis to check if there are any differences in the conductivity of the cathode material.

References

Al-Thyabat, S., Nakamura, T., Shibata, E. & Lizuka, A., 2013. Adaptation of minerals processing operations for lithium-ion (libs) and nickel-metal hydride (NiMH) batteries recycling: Critical review. *Minerals Engineering,* Volume 45, pp. 4 – 17.

Chandra, N., Sharma, V., Chung, G. & Schroder, D., 2011. Four-point characterization of 4H silicon carbide. *Solid-State Electronics,* Volume 64(1), pp. 73 – 77.

Chang, H. & Huang, P. J., 1998. Dehydration of $CuS0_4.5H_20$ Studied by Thermo-Raman Spectroscopy. *Journal of the Chinese Chemical Society,* Volume 45(1), pp. 59 – 66.

Chen, W., Mai ,L.Q., Peng, J. F., Xu, Q & Zhu, Q.Y., 2004. FTIR study of vanadium oxide nanotubes from lamellar structure. *Journal of Materials Science,* Volume 39, pp. 2625 – 2627.

Chen, Y., Feng, H., Wang, Y.,Tang, Z., Chua, D.,2018. Nanoporous copper metal current collector for lithium ion batteries. *Materials Letters,* pp. 8 – 12.

Clark, J. M., Eames, C., Reynaud, M., Rousse,G., Chotard, J.N., Tarascon, J.M., Islam, M.S., 2014. High voltage suphate cathodes $Li_2M(SO_4)_2$ (M = Fe, Mn, Co): Atomic-scale studies of lithium diffusion, surfaces, and voltage trends. *Materials Chemistry A,* Volume 2, pp. 7446 – 7453.

Cullity, B., 1978. *Elements of X-ray Diffraction*. Addison Wesley: Mass.London

Dewulf, J.,Van der Vorst, G., Denturck, K., Van Langenhove, H., Ghyoot, W., Tytgat, J., Vandeputte, K., 2010. Recycling rechargeable lithium ion batteries: Critical analysis of natural resource-saving. *Resource, Conservation, and Recycling,* pp. 229 – 234.

Doadrio, A. L., Sotelo, J. & Fernández-Ruan, A., 2002. Synthesis and characterization of oxovanadium (iv) dithiocarbamates with pyridine. *Quim. Nova, Volume* 25(4), pp. 525 – 528.

Griffiths, P. & de Hasseth, J., 2007. *Fourier transform infrared spectrometry*. Wiley-Blackwell:USA

Gu, F., Guo J., Yao X., Summer, P., Widijatmoko, S., Hall, P., 2017. An investigation of the current status of recycling spent lithium -ion batteries from consumer electronics in China. *Journal of Cleaner Production,* pp. 765 – 780.

Guimond, S.,Haija, M., Kaya, S., Lu, J., Weissenrieder, J., Shaikhutdinov, S., Kuhlenbeck ,H., Freund, H.J., Dobbler, J., Sauer, J., 2006. Vanadium oxide surfaces and supported vanadium oxide nanoparticles. *Topics in Catalysis*, Volume 38, pp. 117 - 125.

Iizuka., Atsushi.Y., Yasunobu, N., Hiroki ,Y., Akihiro., 2013. Separation of lithium and cobalt from waste lithium-ion batteries via bipolar membrane electrodialysis coupled with chelation. *Separation and Purification Technology,* Volume 113, pp. 33 – 41.

Jha, M. K.,Kumari, A., Jha, A.K., Kumar, V., Hait, J., Pandey, B.D., 2013. Recovery of lithium and cobalt from waste lithium ion batteries of mobile phone. *Waste Management,* Volume 33, pp. 1890 – 1897.

Khan, A., Rashid, A., Younas, R. & Chong, R., 2016. A chemical reduction approach to the synthesis of copper nanoparticles. *International Nano Letters,* Volume 1, pp. 21 – 26.

Kovachev,G., Schrottner, H.,Aiello, L.,Hanzu, L., Wilkening. H.M.,Foitzik, A.,Wellm, M., Sinz, W., Ellersdorfer, C., 2019. Analytical Dissection of an automotive Li-Ion Pouch cell. Batteries, Volume 5(4), PP.1-67.

Kusuma, M. & Chandrappa, G. T., 2019. Effect of Calcination Temperature on characteristic properties of $CaMoO_4$ nanoparticles. *Journal of Science: Advanced Materials and Devices,* 4(1), pp. 150 – 157.

Lander, L., Reynaud, M., Carrasco, J., Katcho, N.A., B, C., Polian, A., Baptiste, B., Rousse, G., Tarascon, J.M., 2016. Unveiling the electrochemical mechanisms of $Li_2Fe(SO_4)_2$ polymorphs by neutron diffraction and density functional theory calculations. *Physical Chemistry Chemical Physics,* pp. 14509 – 14519.

Lander, L., Reynaud, M., Rousse, G., Sougrati, M.T., Robert, C.L., Messinger, R.J., Deschamps, M., Tarascon, J.M., 2014. Synthesis and Electrochemical Performance of the Orthorhombic $Li_2Fe(SO_4)_2$ Polymorph for Li-ion Batteries. *Chemistry of Materials,* Volume 26, pp. 4178 – 4189.

Laura, L., 2016. *Exploration of new sulfate-based cathode materials for lithium ion batteries,* Paris: Ph.D. Thesis.

Levason, W.,Reid, G. & Zhang, W., 2014. Synthesis, Properties, and Structures of Chromium(vi) and Chromium(v) Complexes with Heterocyclic Nitrogen Ligands. *Anorganische und Allgemeine Chemie,* pp. 35 – 39.

Liu,H., Wu,Y.O., Rahm, E., Holze. R., Wu, H. Q., 2004. Cathode materials for lithium ion batteries prepared by Sol-gel methods. *Journal of Solid State and Electrochemistry* pp. 450 – 466.

Ma, L., Xiaoping, Z., Limei, X., Xuyao, X., Lingling, Z., Weixiang, C., 2015. Chitosan-assisted fabrication of ultrathin MoS_2/graphene heterostructure for Li-ion battery with excellent electrochemical performance. *Electrochimica Acta,* Volume 167, pp. 39 – 47.

Mayyas, A., Steward, D. & Mann, M., 2018. The case for recycling: Overview and challenges in the material supply chain for automotive Li-ion batteries. *Sustainable Materials and Technologies,* Volume 17, pp. 1 – 26.

Nitta, N., Wu, F., Lee, J. T. & Yushin, G., 2015. Li-ion battery materials: present and future. *Material Today,* Volume 18, pp. 252 – 264.

Oliveira, L., Messagie, M., Rangaraju, S., Sanfelix, J., Rivas, M.H., Mierlo, J.V., 2015. Key issue of lithium-ion batteries - from resource depletion on to environmental performance indicators. *Journal of Cleaner Production,* Volume 108, pp. 354-362.

Petersen, C. L.,Hansen, T.M., Boggild, P., Boisen, A., Hansen, O., Hassenkam, T., Grey, F., 2002. Scanning microscopic four-point conductivity probes. *Sensors and Actuators A Physical,* volume 96(1), pp. 53 – 58.

Prabaharan, G., Barik, S. p., Kumar, N. & Kumar, L., 2017. Electrochemical process for electrode material of spent lithium-ion batteries. *Waste Management,* Volume 68, pp. 527 – 533.

Qiao, H., Wei, Z., Yang, H., Zhu, L. & Yan, X., 2009. Preparation and Characterization of NiO particles by Anodic Arc Plasma Method. *Journal of Nanomaterials,* Article ID 795928, 5 pages.

Radha, A. V., Lander, L., Rousse, G., Tarascon, J. M., Navrotsky, A., 2015. Thermodynamic stability and correlation with synthesis conditions, structure, and phase transformations in

orthorhombic and monoclinic $Li_2M(SO_4)_2$ (M = Mn, Fe, Co, Ni) polymorphs. *Journal of Materials Chemistry A,* Volume 3, pp. 2601 – 2608.

Reynaud, M., 2014. *Design of new sulphate - based positive electrode materials for Li- and Na-batteries,* PhD thesis, Université de Picardie Jules Verne, France. [https://tel.archives-ouvertes.fr/tel-01018912/document, accessed on 18.06.2020]

Reynaud,M.,Rodríguez-Carvajal,J.,Chotard,J.,Tarascon,J.M .,& Rousse, Gwenaëlle.,2014. Magnetic structure and properties of orthorhombic $Li_2Ni(SO_4)_2$. *Physical Review B,* Volume 89, pp. 104419-1 - 104419-9.

Satyavani, T. V., Kumar, A. S. & Rao, P. S., 2015. Methods of synthesis and performance improvement of lithium iron phosphate for high rate Li-ion batteries: A review. *Engineering Science and Technology, International Journal,* Volume 19, pp. 178 – 88.

Schwieger, J. N., Kraysberg, A. and Ein-Eli, Y., 2011. Copper sulfates as cathode materials for lithium batteries. *Journal of Power Sources,* Volume 196(3), pp. 1461 – 1468.

Stokes, J. D., 2008. *Principles and Practice of Variable Pressure Environmental Scanning Electron Microscopy.* John Wiley & Sons: United Kingdom

Theivasanthi, T. & Alagar, M., 2010. X-Ray Diffraction Studies of Copper Nanopowders. *Archives of Physics Research,* Volume 1(2), pp. 112 – 117.

Valdes, L., 1954. Resistivity Measurements on Germanium for Transistors. *Proceedings of the I.R.E,* Volume 42(2), pp. 420 – 427.

Xi, Guoxi; Xu, Huidao; Yao Lu., 2015. Study on preparation of NiCo ferrite using spent lithium-ion and nickel-metal hydride batteries. *Separation and Purification Technology,* Volume 145, pp. 50 – 55.

Yi, T.-F.; Jie, M. & Zhu,Y.-R., Z., 2016. Key strategies for enhancing the cycling stability and rate capacity of $LiNi_{0.5}O_4$ as high-voltage cathode materials for high power lithium-ion batteries. *Journal of Power Sources,* Volume 316, pp. 85 – 105.

Zhuang, H., Xu, Y., & Zhao, P., 2020. Effect of crystallinity on capacity and cyclic stability of $Na_{1.2}V_3O_{7.9}$ nanoplates as lithium-ion cathode materials. *Journal of Solid State Electrochemistry*, Volume 24, pp. 217 – 223.

Appendix

Table 1: Summary of FTIR spectral data of $Li_2Cu(SO_4)_2$ calcined at 500°C for 3 h for both sol-gel and solid-state method

Functional groups	Solid-state $Li_2Cu(SO_4)_2$ calcined at 500 °C for 3 h Wavenumber (cm^{-1})	Solid-state $Li_2Cu(SO_4)_2$ calcined at 500 °C for 7 h Wavenumber (cm^{-1})	Sol-gel method. $Li_2Cu(SO_4)_2$ calcined at 500 °C for 3 h Wavenumber (cm^{-1})	Sol-gel $Li_2Cu(SO_4)_2$ calcined at 500 °C for 7 h Wavenumber (cm^{-1})
Li-O	410.27	none	460.	none
O-H bending	608.43, 1611.79	616.75, 1631.48	651.74, 1611.70	651.12, 1631.48
S-O stretching	1098.84	1094.28	1104.48	1094.28
C-O	1611.70	1610.96	1611.79	1610.96

Table 2: Summary of FTIR spectral data of Li_2CrSO_4 calcined at 500 °C for 3 h for both sol-gel and solid-state method

Functional groups	Solid-state Li_2CrSO_4 calcined at 500 °C for 3 h Wavenumber (cm^{-1})	Solid-state Li_2CrSO_4 calcined at 500 °C for 7 h Wavenumber (cm^{-1})	Sol-gel Li_2CrSO_4 calcined at 500 °C for 3 h Wavenumber (cm^{-1})	Sol-gel Li_2CrSO_4 calcined at 500 °C for 7 h Wavenumber (cm^{-1})
Cr-O stretching	441.26-531, 609.48	441.51-532.38 612.58	532.50 612.34	533.33 612.54
O-H bending	1613.17	1610.72	1609.96	1610.25
S-O stretching	531.	532.28	532.50	533.33
S-O vibration	1114.42	1096.96	1097.31	1097.02

Table 3: Summary of FTIR spectral data of $Li_2VO(SO_4)_2$ calcined at 500 °C for 3h for both sol-gel and solid-state method

Functional groups	Solid-state $Li_2VO(SO_4)_2$ calcined at 500 °C for 3 h Wavenumber (cm^{-1})	Solid-state $Li_2VO(SO_4)_2$ calcined at 500 °C for 7 h Wavenumber (cm^{-1})	Sol-gel $Li_2VO(SO_4)_2$ calcined at 500 °C for 3 h Wavenumber (cm^{-1})	Sol-gel $Li_2VO(SO_4)_2$ calcined at 500 °C for 7 h Wavenumber (cm^{-1})
Li-O			413.40	410.45
O-H bending	1610.96	1614.58	1612.34	1611.08
V=O vibration	935.05-1001.27	1011.06	1012.04	1011.92
S-O stretching	1096.63	1112.36-1151.02	1102.14	1100.88

Table 4: XRD peak indexing of all synthesized compounds

Figure 15a (*r* = 0,205 nm)						Figure 15b (*r* = 0,205 nm) Khan *et al* (2016)					
2θ	**d (nm)**	**Intensity**	**a (nm)**	**a^2/d^2**	***hkl***	**2θ**	**d (nm)**	**Intensity**	**a (nm)**	**a^2/d^2**	***hkl***
44	0,206	400	0,580	9	300	44	0,206	400	0,580	9	300
Figure 16a (*r* = 0,205 nm)						Figure 16b (*r* = 0,205 nm) Khan *et al* (2016)					
44	0,206	360	0,580	9	300	44	0,206	440	0,580	9	300
Figure 17a (*r* = 0,128 nm)						Figure 17b (*r* = 0,205 nm) Khan *et al* (2016)					
42	0,215	480	0,362	4	200	36	0,250	480	0,362	1	100
54	0,170	360	0,362	4	200	42	0,215	400	0,362	4	200
Figure 18a (*r* = 0,128 nm)						Figure18b (*r* = 0,205 nm) Khan *et al* (2016)					
44	0,206	480	0,362	4	200	54	0,170	300	0,362	4	200
54	0,170	350	0,362	4	200						
Figure19a (*r* = 0,128 nm)						Figure19b (*r* = 0,205 nm) Khan *et al* (2016)					
40	0,226	1200	0,362	4	200						
Figure 20a (*r* = 0,128 nm)						Figure 20b (*r* = 0,205 nm) Khan *et al* (2016)					
40	0,226	1400	0,362	4	200						

Table 5: Comparison of SEM results between sol-gel and solid-state

Compound	Calcination temperature & Time	Solid-state route particle size	Sol-gel route particle size	Reference Figure number
$Li_2Cu(SO_4)_2$	500 °C for 3 h	Larger	Smaller	Figure 24
$Li_2Cu(SO_4)_2$	500 °C for 7 h	Slightly larger	Slightly smaller	Figure 21
Li_2CrSO_4	500 °C for 3 h	Larger	Smaller	Figure 25
Li_2CrSO_4	500 °C for 7 h	Larger	Smaller	Figure 22
$Li_2VO(SO_4)_2$	500 °C for 3 h	Larger	Smaller	Figure 26
$Li_2VO(SO_4)_2$	500 °C for 7 h	Larger	Smaller	Figure 23